Component-Oriented Modeling of Thermoelectric Devices for Energy System Design

Felix Felgner, *Member, IEEE*, Lukas Exel, Marco Nesarajah, and Georg Frey, *Senior Member, IEEE*

***Abstract*—Thermoelectric (TE) devices are used in the form of Peltier coolers and as TE generators, with the latter producing electrical energy from waste heat, based on the Seebeck effect. In both cases, modeling of the TE device is a prerequisite for the design and control verification of the resulting overall energy system. To this end, the model has to be integrated seamlessly in an overall system model containing other electrical, thermodynamic, or even mechanical components. Following this premise, this paper presents a component-based model for TE devices described in the Modelica language. The model incorporates the temperature dependences of decisive material properties (Seebeck coefficient, thermal conductivity, and electrical resistivity) in 1-D spatial resolution. With the help of few additional geometrical parameters, e.g., the thickness of TE legs, the model is capable of describing the dynamic behavior of the TE device in accordance with the experimental results.**

***Index Terms*—Component-oriented modeling, energy efficiency, Modelica, Peltier cooler, simulation, thermoelectric (TE) devices, thermoelectric generator (TEG), thermoelectricity, waste heat recovery.**

I. Introduction

A THERMOELECTRIC (TE) power device can be designed as a TE generator (TEG) in order to generate electric power from a heat flow. It may also be designed in the reverse sense, i.e., in a large variety of applications, as a Peltier cooler or, more particularly, as a fine-scale spatially distributed heating and cooling device (e.g., in lithography [1]). In all applications, TE devices show specific characteristics in which they differ from classical thermal machines: mechanical simplicity (due to the lack of moving parts), uncomplicated scalability of size, and low-maintenance operation as well as very high reliability and durability, which have been proven for several decades during space missions.

Today's increasing demand in energy saving, along with advances in TE material qualities and considerably reduced production costs, has promoted the attractiveness of TE technologies. This is especially true for TEGs, where various new application-oriented design efforts are being made. They range from energy harvesting for small wireless sensors [2]–[6] to the recovery of larger amounts of waste heat from the exhaust of combustion engines [7]–[11], from heat-intensive metal production [12], and from very particular processes like biomass drying [13], for example. Summaries of recent developments, patents, and applications in waste heat recovery are given in [14] and [15], and advances in TE material science are given in [16] and [17]; a precise measurement system for TE material properties is described in [18].

Despite their low efficiency, especially at moderate heat supply temperatures, the use of TEGs can be worthwhile where a notable amount of waste heat is available for free. In this spirit, TE waste heat recovery is commonly regarded as a renewable source [15]. In the high power and temperature range, however, the overall benefit of TEGs is still contentious, as argued in [19], for instance.

A. Modeling of TE Power Devices for System Design

In most applications, the TE device is part of a *system* where it interacts with its thermal and electrical boundary components. Several generalized design considerations for typical applications and boundary conditions have been recently reported, e.g., concerning the qualification of TE materials [20], optimal dimensions [21], or the heat transfer conditions around the TE device [22], [23]—although based on simplified lumped TE models. It is desirable to *model* and *simulate* the specific whole-system behavior for an optimal design. In all of the aforementioned reported works, the TE phenomena are integrated into the respective considerations, based on simplified, steady-state, and lumped equations (requiring appropriately averaged material data). They do not aim to provide a *versatile* and *reusable TE component model* and, consequently, do not address model implementation. Such a component model should be as generic as possible, i.e., applicable to possibly any TE module via individual parameterization and thereby *integrable* into a complex *system model*. This will succeed most conveniently in an established all-purpose modeling and simulation environment such as MATLAB/Simulink or Dymola/Modelica.

Reference [24] describes implementations of TEG and Peltier cooler models in MATLAB/Simulink; the models are fully lumped (i.e., operate with averaged material properties), describe steady-state conditions, and, following Simulink's signal-oriented scheme, have a unidirectional input/output causality. Reference [25] also mentions (with few details) the implementation of a transient model by a Simulink S-Function; the restricted interactions with other physical models due to the causal interfaces, however, remain. In [26], [27], and [28], by contrast, SPICE-compatible equivalent circuits of TE modules are presented (in [26] and [28] for steady-state and transient conditions, and in [27] for steady state only), showing good agreement with laboratory experiments, although the SPICE

Manuscript received December 11, 2012; revised March 11, 2013; accepted April 7, 2013. Date of publication May 1, 2013; date of current version August 23, 2013.

The authors are with the Chair of Automation, Saarland University, 66123 Saarbrücken, Germany (e-mail: felix.felgner@aut.uni-saarland.de).

Color versions of one or more of the figures in this paper are available online at http://ieeexplore.ieee.org.

Digital Object Identifier 10.1109/TIE.2013.2261037

implementation makes is necessary to emulate all nonelectrical processes by analogies from the electrical domain—inside the TE model as well as in the model of the incorporating energy system.

B. Contribution of This Paper

This paper offers an intrinsic *multidomain model* for TE devices. The model is based on the draft outlined in [30], which is now elaborated in detail, enhanced, and examined. The objective of the model is not only to help evaluate existing TE products. The model should also support the conception and verification of completely new system designs, based on the *dimensions* of the TE elements applied and the *essential physical material properties*: Seebeck coefficient, thermal conductivity, and electric resistivity. All of those properties are significantly dependent on temperature for common TE materials and, consequently, vary within a TE leg which is subject to a steep temperature gradient. Averaged properties given in product datasheets are only valid under default thermal conditions; calculating average values from the arithmetic mean of the cold-side and hot-side temperatures requires steady-state conditions and property curves being sufficiently linear in the temperature range.

The model presented is implemented in the open Modelica modeling language [31], [32] which has often been proven as a proper technique in the modeling of thermopower systems, e.g., in [33] and [34]. The component-oriented modeling with *noncausal interfaces* ("connectors") preserves the physical system structure and allows a straightforward system model construction out of reusable components. This includes, for instance, the (re-)use of sophisticated heat exchangers models, which are crucial for a proper system design. Such Modelica heat exchanger models have already been demonstrated and applied in the context of TE devices [10], [35]. In fact, these works emphasize the peripheral components, while the used TE device models are static, based on lumped equations for the TE voltage and the external heat flows.

This contribution, by contrast, focuses on the generic modeling of TE elements. Section II starts by providing the partial differential equations which govern the behavior of a 1-D TE leg. Thereupon, a generic Modelica model is developed, and it is explained how to construct a complete TE device model. The example in Section III shows a TEG model integrated into thermal and electric boundaries and compares its simulation results with those of a simpler commonly applied model. Section IV validates the Modelica model on the basis of experimental data. A summarizing conclusion and an outlook are given in Section V.

II. Mathematical Model of TE Device

A. Essential Equations

The TE material behavior is considered in a straightforward physical manner. The core component represents a piece of TE material, which is a small segment cut out of a 1-D TE leg with length L. This segment is the base of an arbitrary TE device and may be a p-doped or n-doped semiconductor as well as any TE conductor. The segment has (average) temperature T, length dx, cross-sectional area A, its center located at position x, and electrical current I in the positive direction of x [cf., Fig. 1(a)]. Then, the *electrical behavior* is given by the thermal voltage dU_{th} and the voltage drop dU_R due to the material resistance dR

$$dU = dU_{\mathrm{th}} - dU_R = \alpha\left(-\frac{\partial T}{\partial x}\right)dx - dR \cdot I. \tag{1}$$

The inner *thermal behavior* results from an energy balance known from literature, e.g., [38] (with different notation)

$$\underbrace{c\rho\frac{\partial T}{\partial t}Adx}_{\substack{\text{Derivative of}\\ \text{internal energy}}} = \underbrace{-\frac{\partial}{\partial x}\left(-\lambda\frac{\partial T}{\partial x}\right)Adx}_{\substack{=:d\dot{Q}_C\\ \text{Heat absorption}\\ \text{due to conduction}}} \underbrace{-IT\frac{\partial \alpha}{\partial x}dx}_{\substack{=:d\dot{Q}_T\\ \text{Heat absorption}\\ \text{due to Thomson effect}}} + \underbrace{I^2\overbrace{\frac{r}{A}dx}^{dR}}_{\substack{=:d\dot{Q}_J\\ \text{Joule heat}\\ \text{production}}} \tag{2}$$

where

$$T\frac{\partial \alpha}{\partial x} = T\frac{\partial \alpha}{\partial T}\frac{\partial T}{\partial x} = \tau\frac{\partial T}{\partial x} \tag{3}$$

with

- α Seebeck coefficient;
- λ thermal conductivity;
- r electrical resistivity;
- ρ mass density;
- τ Thomson coefficient;
- t time;
- c specific (isobaric) heat capacity.

In other literature, the heat absorption related to the Thomson effect is often neglected (corresponding to a temperature-independent Seebeck coefficient). Reference [29] shows an example where the Thomson effect clearly affects the output voltage of a TEG. In order to devise the following models as generally as possible, the Thomson effect is kept. Its representation in (2), i.e., by means of the spatial derivative of the Seebeck coefficient $\partial\alpha/\partial x$ instead of the Thomson coefficient $\tau := T \cdot \partial\alpha/\partial T$ spares providing the Thomson coefficient, either from literature or by numerically differentiating α curves with respect to T. Therefore, the effect will not complicate the model parameterization. Equation (2) does not display the conductive nor the Peltier heat flows on the segment's boundaries; those heat flows will appear in the implementation with finite spatial discretization (Section II-B). The energy balance includes an emitted *electrical power* dP_{el}

$$dP_{\mathrm{el}} = dU \cdot I \overset{(1)}{=} \overbrace{\alpha\left(-\frac{\partial T}{\partial x}\right)dx \cdot I}^{dP_{\mathrm{th}}} - \overbrace{dR \cdot I^2}^{d\dot{Q}_J} = dP_{\mathrm{th}} - d\dot{Q}_J. \tag{4}$$

The first term on the right side of (4) (dP_{th}) is the electric power which is related to the TE material behavior. The second term $d\dot{Q}_J$ is the Joule heat production; it reduces the actually

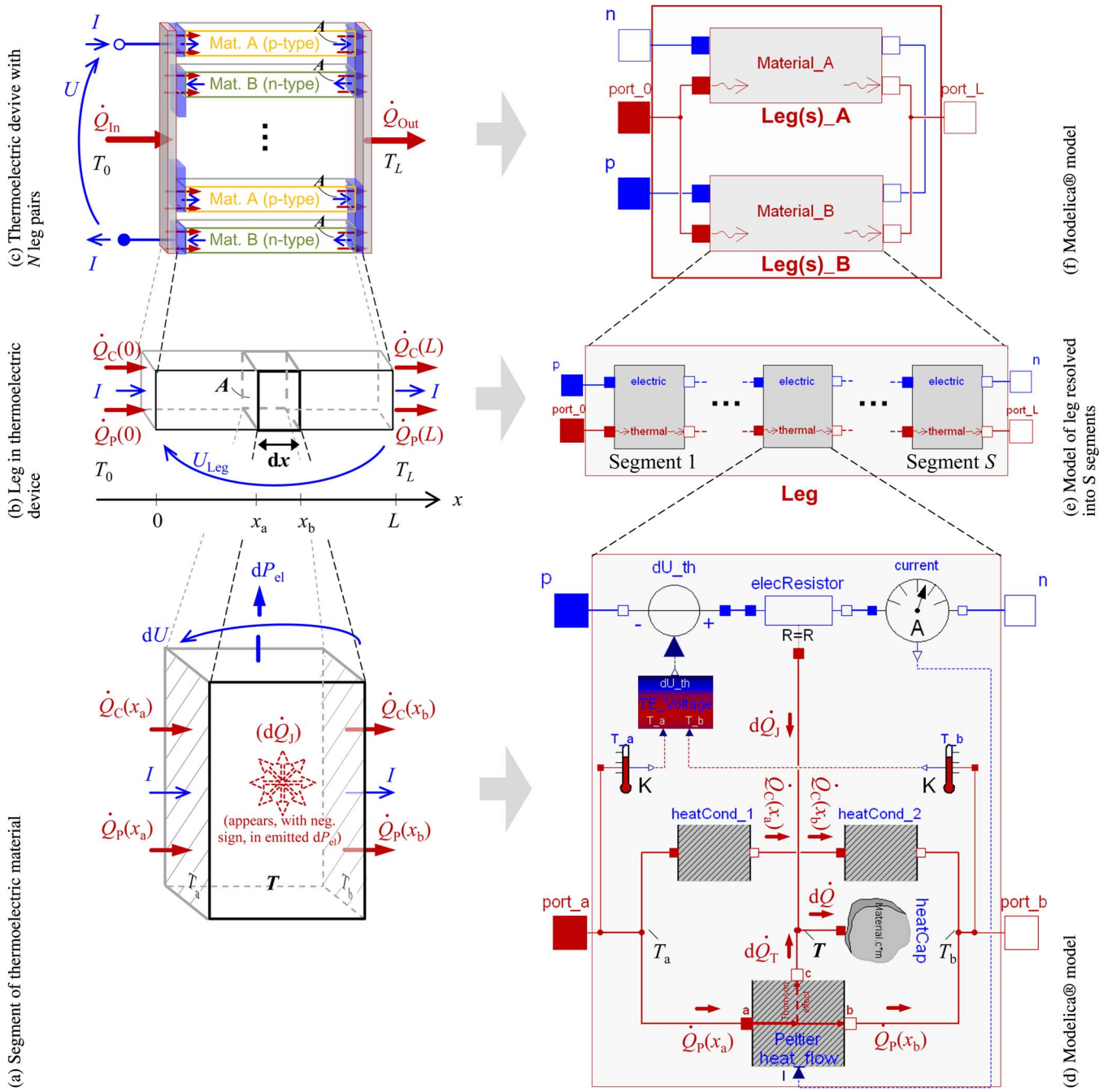

Fig. 1. TE device. (a) Segment of TE material with energy flows. (b) One-dimensional TE leg. (c) TEG or Peltier cooler. (d) Modelica model diagram of TE segment. (e) Model of TE leg. (f) Model of TE couple (parameterized to represent TE device with N leg couples).

emitted power. That is, via dP_{el}, the incoming and outgoing energy flows in Fig. 1(a) already respect the Joule heat production. From this external point of view, $d\dot{Q}_J$ does not arise from an additional inner source [and therefore, it is bracketed in Fig. 1(a)].

Based on the aforementioned relations, the *dynamics* of the TE material behavior are as follows:

1) *thermally transient*;
2) *electrically static*, i.e., no electrical capacities and inductivities are considered inside the TE material;
3) *electronically static*, i.e., the electrical potential caused by TE charge displacement responds to the thermal conditions without delay.

The temperature profile in the model has *1-D spatial resolution*, i.e., $T = T(x,t)$. It is this spatial resolution that is necessary to directly respect the temperature dependence of the decisive material properties

$$\alpha = f_\alpha\left(T(x,t)\right) \tag{5a}$$

$$\lambda = f_\lambda\left(T(x,t)\right) \tag{5b}$$

$$r = f_r\left(T(x,t)\right). \tag{5c}$$

The temperature dependence of the specific heat capacity is not considered. This is often less pronounced and affects only the transient behavior. Furthermore, unlike for $\alpha(T)$, $\lambda(T)$, and $r(T)$, curves for $c(T)$ are seldom at hand for TE materials.

B. Component-Oriented Implementation (TrDP Model)

Equations (1) and (2) assume an infinitesimal segment length dx. To build an implementable Modelica model—where only time derivatives may appear explicitly—dx must have a finite size, and the derivatives of T and α with respect to x are approximated by finite differences. (With the limit $dx \to 0$, the following approximations will exactly converge to the partial differential equations from the previous section. The model keeps the "d" for correspondence in front of those quantities that become infinitesimal with the above limit.)

In the construction of a model [Fig. 1(d)] which represents a TE material segment [Fig. 1(a)], several existing components can be reused from the free Modelica standard libraries [31]. This is true for the electrical connectors, "p" and "n" (with electrical potential and current), thermal connectors, "port_a" and "port_b" (with temperature and total heat flow rate), voltage source ("dU_th"), and heat capacitor ("heatCap"). The electrical resistor ("elecResistor") and the heat conductor ("heatCond_1" and "heatCond_2") are modified in order to include the temperature dependence of the material properties. New is the central component "Peltier_heat_flow" describing the Peltier heat flow, including the Thomson effect.

Regarding the *electrical behavior*, the spatial differentiation in (1) is approximated by a finite difference, while the voltage drop dU_R is provided by the resistor model connected in series with the voltage source

$$dU_{\mathrm{th}} = \overline{\alpha} \cdot (T_a - T_b) \qquad (\text{'TE\_Voltage', 'dU\_th'}) \quad (6)$$

$$dU_R = \underbrace{f_r(T) \cdot \frac{dx}{A}}_{dR} \cdot I \qquad (\text{'elecResistor'}). \quad (7)$$

Here, $\overline{\alpha}$ is an averaged value of the Seebeck coefficient, calculated from the distinguished temperatures in the segment T_a, T, and T_b or from a subset of them, e.g., $\overline{\alpha} := (f_\alpha(T_a) + f_\alpha(T_b))/2$, $\overline{\alpha} := (f_\alpha(T_a) + f_\alpha(T) + f_\alpha(T_b))/3$, $\overline{\alpha} := f((T_a + T_b)/2)$, etc., are meaningful possible definitions; depending on the problem considered, they may provide differing accuracies of the modeled dU_{th}. In Section II-C, an alternative of (6) will be introduced, which solves the dilemma of an appropriate average.

Implicitly, the thermal voltage source described by (6) already involves the supply of the TE power dP_{th} as defined in (4). This has to be taken cared of when the Peltier heat flows, which actually feed dP_{th}, are balanced.

For the *thermal behavior* [cf., (2)], the balance of the energy flows depicted in Fig. 1(a) is considered. This balance is reproduced by the model in Fig. 1(d): the left-hand side of (2) is provided by the known heat capacitor model ("heatCap")

$$\underbrace{c\rho A dx}_{=:dC} \frac{dT}{dt} = \underbrace{d\dot{Q}_J + \dot{Q}_C(x_a) - \dot{Q}_C(x_b) + d\dot{Q}_T}_{d\dot{Q}} (\text{'heatCap'}). \quad (8)$$

The Joule heat $d\dot{Q}_J$ [cf., (4)], i.e., the part of dP_{th} not emitted in electric form, is calculated in the resistor model

$$d\dot{Q}_J = f_r(T) \cdot \frac{dx}{A} \cdot I^2 \qquad (\text{'elecResistor'}) \quad (9)$$

and injected into the thermal node to which the TE segment's heat capacitance ("heatCap") is connected [cf., Fig 1(d)].

The heat absorption related to conduction $d\dot{Q}_C = \dot{Q}_C(x_a) - \dot{Q}_C(x_b)$ is modeled by two heat conductors, each representing the conductance of one half of the TE segment. This is an established procedure, e.g., see [32, p. 124] and [39], to which the temperature dependence of λ is added

$$\dot{Q}_C(x_a) = \overbrace{f_\lambda\left(\frac{T_a + T}{2}\right) A}^{=:dG_{\mathrm{left}} \cdot \frac{dx}{2}} \cdot \overbrace{\frac{(T_a - T)}{dx/2}}^{\approx -\partial T/\partial x|_{\mathrm{left}}} \qquad (\text{'heatCond\_1'}) \quad (10a)$$

$$\dot{Q}_C(x_b) = \underbrace{f_\lambda\left(\frac{T + T_b}{2}\right) A}_{=:dG_{\mathrm{right}} \cdot \frac{dx}{2}} \cdot \underbrace{\frac{(T - T_b)}{dx/2}}_{\approx -\partial T/\partial x|_{\mathrm{right}}} \qquad (\text{'heatCond\_2'}) \quad (10b)$$

where $\dot{Q}_C(x_a)$ is the conductive heat flow through the left boundary of the segment and $\dot{Q}_C(x_b)$ is the conductive heat flow through the right boundary. Likewise, $(T_a - T)/(dx/2)$ and $(T - T_b)/(dx/2)$ approximate $-\partial T/\partial x$ (inner derivative of $d\dot{Q}_C$ term in (2)) in the left and right halves, respectively.

The "Peltier_heat_flow" component must also provide appropriate heat flows on the TE segment's boundaries (which superpose with the conductive heat flows in the thermal connectors). They are assigned to the connectors "a" and "b" [cf., Fig. 1(d)]

$$\dot{Q}_P(x_a) = \overbrace{f_\alpha(T_a)}^{=:\alpha_a} \cdot T_a I \qquad (\text{'Peltier\_heat\_flow'}) \quad (11a)$$

$$\dot{Q}_P(x_b) = \underbrace{f_\alpha(T_b)}_{=:\alpha_b} \cdot T_b I \qquad (\text{'Peltier\_heat\_flow'}). \quad (11b)$$

In addition, "Peltier_heat_flow" defines $d\dot{Q}_T$ (assigned to the central connector "c"), the Thomson-effect-related heat flow absorbed by the segment's heat capacitance. "Peltier_heat_flow" is not split like the heat conductance. On the one hand, this is due to the different mathematical structure ($d\dot{Q}_T$ in (2) results from a first spatial derivative and not from a second one as $d\dot{Q}_C$). On the other hand, part of the difference $\dot{Q}_P(x_a) - \dot{Q}_P(x_b)$ provides the electrical power dP_{th} associated with the thermal voltage, and dP_{th} was already implicitly included in the voltage source [cf., (6)]. Therefore, $d\dot{Q}_T$ is the residual of $\dot{Q}_P(x_a) - \dot{Q}_P(x_b) - dP_{\mathrm{th}}$

$$\begin{aligned} d\dot{Q}_T &= \dot{Q}_P(x_a) - \dot{Q}_P(x_b) - \overbrace{dU_{\mathrm{th}} I}^{dP_{\mathrm{th}}} \qquad (\text{'Peltier\_heat\_flow'}) \\ &\overset{(11),(6)}{=} (\alpha_a T_a - \alpha_b T_b)\, I - \alpha_c\,(T_a - T_b)\, I \\ &= [(\alpha_a - \alpha_C) T_a - (\alpha_b - \alpha_c) T_b]\, I \\ &= - \underbrace{\frac{1}{2}\left(\underbrace{\frac{\alpha_c - \alpha_a}{dx/2} T_a}_{\approx T \cdot \frac{\partial \alpha}{\partial x}|_{\mathrm{left}}} + \underbrace{\frac{\alpha_b - \alpha_c}{dx/2} T_b}_{\approx T \cdot \frac{\partial \alpha}{\partial x}|_{\mathrm{right}}}\right)}_{\approx T \cdot \partial\alpha/\partial x \quad \text{(average of left and right half)}} I \cdot dx \end{aligned} \quad (12)$$

with $\alpha_c := f_\alpha(T)$ as the Seebeck coefficient at the central connector "c"; $\alpha_c = \overline{\alpha}$ or $\alpha_c \approx \overline{\alpha}$ depending on the definition chosen for $\overline{\alpha}$.

The last two manipulations of the right-hand side of (12) show that the aforementioned implementation is a meaningful and consistent approximation of the Thomson-effect-related heat absorption in the original partial differential equation (2). Given a temperature gradient in the TE segment, $d\dot{Q}_T$ occurs only if the Seebeck coefficient is temperature dependent. According to (3), this is equivalent to a Thomson coefficient $\tau \neq 0$. The *temperature-dependent* functions of the *material properties* (5) can be included by means of interpolated lookup tables. When the model is used for system design, the tables can be conveniently filled with the data delivered from the TE material manufacturer.

The *series connection* of S instances of the TE segment model from Fig. 1(d) represents a 1-D discretized TE leg with length L and cross section A [Fig. 1(b) and (e)]. This is the final implementation of the original equations (1) and (2) with S intermediate temperatures $T(x_i)$ at positions

$$x_i = \frac{L}{S}\left(i - \frac{1}{2}\right), \qquad i = 1, \ldots, S \tag{13}$$

and S segment voltages dU_i.

Due to the undirected connector variables, the segment models operate interactively. The electrical and thermal segment resistances are piled up, as well as the voltages: $U_{\mathrm{Leg}} = \sum_i dU_i = \sum_i -\alpha(T(x_i))dT_i - dR_i I$, with $dT_i = T_{b,i} - T_{a,i}$, is a numerical integration of (1). For further reference, the model defined by (5)–(12) is called the transient distributed-properties model (TrDP model).

C. Model Refinement for Extreme Temperature Profiles (TrDP$_{\alpha\mathrm{Int}}$ Model)

Based on (5)–(12) from the preceding section, the TE leg model is complete. With its spatial discretization, the behavior is emulated at S equidistant sampling points alongside the temperature profile from T_0 to T_L. However, regarding the transient behavior, extreme situations where (nearly) the entire temperature difference $T_0 - T_L$ falls upon one single leg segment (even if its finite length $dx = L/S$ is chosen very small) are possible. This will be the case in a step-response-like startup. For instance, the TE leg, which was initially in thermal equilibrium with the ambience, is suddenly exposed to a higher temperature at its left end ($x = 0$). Then, in the early transient phase, the temperature profile may look as depicted in Fig. 2: almost the entire TE voltage U_{th} is generated in segment 1 (while the ohmic voltage drop is still distributed over all segments).

According to (6), the total voltage U_{Leg} is effectively calculated based on the Seebeck coefficient value $\overline{\alpha}$ defined for segment 1. With the temperatures T_a, T, and T_b differing that much in this single segment, it is hardly possible to define an averaged $\overline{\alpha}$ appropriate for any material characteristics $\alpha(T)$.

This dilemma can be solved by eliminating the spatial coordinate x from the calculation of dU_{th} [cf., (1)], which means that dU_{th} ultimately only depends on the integral of $\alpha(T)$ within the respected temperature interval (see gray shaded areas in Fig. 2). To accomplish this in the TE segment model, the tabulated material properties from (5) are supplemented by

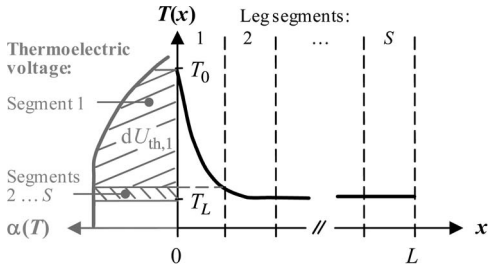

Fig. 2. Extreme transient temperature profile, e.g., in the initial phase of the step response.

$$V = f_V(T) := \int_{T_{\min}}^{T} \alpha(\vartheta)\, d\vartheta \tag{14}$$

which is preferably determined offline from the $\alpha(T)$ data. The quantity V is the TE voltage generated in the respected material between the temperatures $T_{\min}$ and T—independently of the local profile $T(x)$ ($T_{\min}$ is the minimal temperature appearing in the $\alpha(T)$ data.). Equation (6) is then replaced by

$$dU_{\mathrm{th}} = f_V(T_a) - f_V(T_b) \quad (\text{'TE\_Voltage'}, \text{'dU\_th'}) \tag{15}$$

where $T_a, T_b \geq T_{\min}$.

Refined by integrals of $\alpha(T)$, the segment model defined by (5), (7)–(12), (14), and (15) shall be named the TrDP α-integrals model (TrDP$_{\alpha\mathrm{Int}}$ model). The effect of the refinement is discussed in Section III.

D. Building TE Device Model

A TE device usually consists of several couples of legs. Each couple contains a p-doped leg ($\alpha > 0$, "Leg_A") and an n-doped leg ($\alpha < 0$, "Leg_B") which are thermally in parallel and electrically in series. Hence, the legs' TE voltages add up. Fig. 1(f) shows the corresponding model. Typically, all couples are arranged thermally in parallel and electrically in series.

With the number of couples N often being larger than 100, a device model containing hundreds of legs, each with S intermediate temperatures as states, becomes numerically expensive ($2N \cdot S$ states). However, the number of states can be reduced to just 2 S if all the legs are thermally in parallel and have the same current I: all A legs can be merged to one A leg, and all B legs can be merged to one B leg. Then, only one couple remains in the model, as shown in Fig. 1(f). In order to obtain the correct resultant electrical resistances, thermal conductances, and thermal capacities, the parameter N is inserted already on the level of the segment model: the electrical resistance (dR_i), the two half thermal conductances (dG_i^{left} and dG_i^{right}), and the heat capacitance (dC_i) of the segment model are multiplied by N. This corresponds to adding the factor N on the left-hand side of (8) and on the right-hand side of (6) or (15), respectively, (7), and (9) to (12) [cf., Fig. 1(c) and (f)]. On the top level, a TEG or Peltier cooler model can be parameterized via the interface shown in Fig. 3.

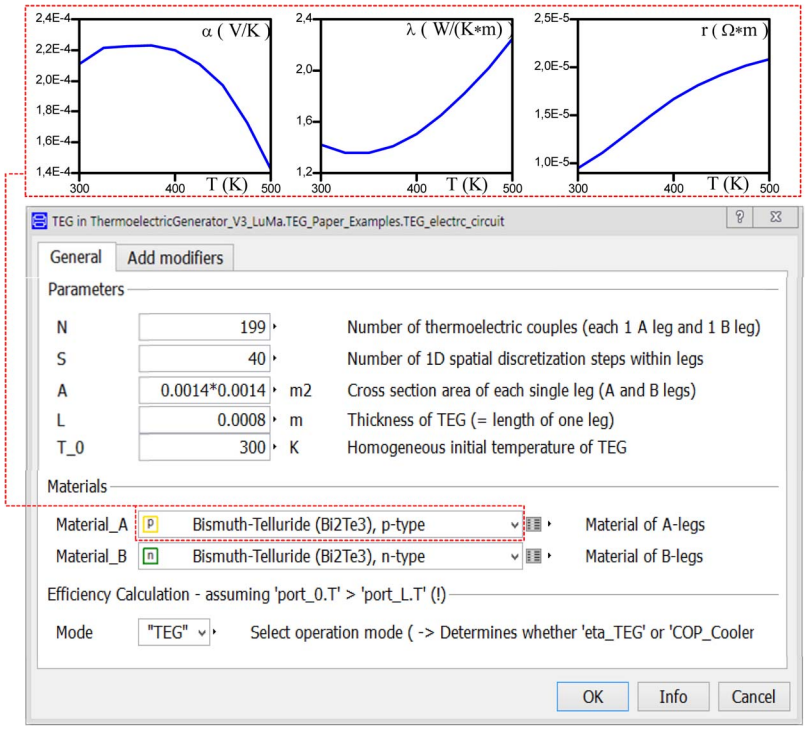

Fig. 3. Parameter table of the Modelica model of TE device (TEG), parameterized with bismuth-telluride material properties provided by [41].

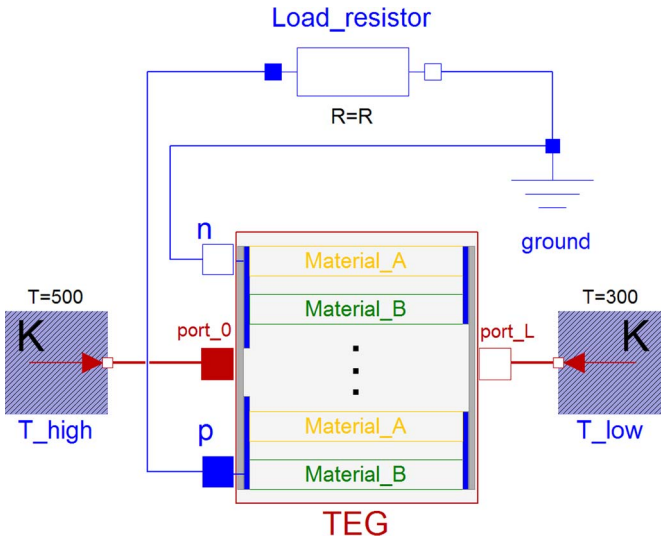

Fig. 4. Modelica model of TEG according to Section II (Fig. 1(f), connected to load resistor and thermal boundaries).

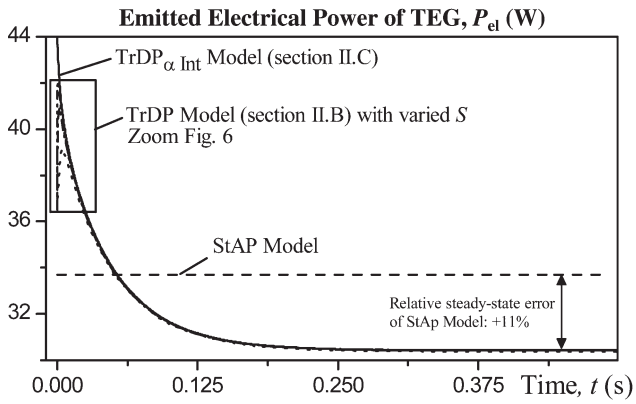

Fig. 5. Simulation of system model from Fig. 4 ($T_{\mathrm{high}} = \mathbf{500}$ K and $T_{\mathrm{low}} = 300$ K): notable transient and steady-state deviations between the TrDP/TrDP$_{\alpha\mathrm{Int}}$ model and the StAP model (setting 1).

The genericity of the basic TE segment model also allows the simple construction of advanced TE devices, such as *cascaded* or *segmented* TEGs [40]. These devices can achieve higher efficiency by connecting different materials thermally in series. The presented Modelica can simulate such devices (based on arbitrary given temperature curves of the material properties) and can help in optimizing specific free parameters.

III. Example: Simulation of TEG

To illustrate the usage of the derived models, a TEG feeding an electric load is considered. The TEG has $N = 199$ couples with p- and n-doped bismuth-telluride ($\mathrm{Bi_2Te_3}$) (cf., parameter table in Fig. 3). Fig. 4 shows the intuitively constructible Modelica diagram of the system. The simplicity of the TEG's thermal boundaries (with constant temperatures $T_{\mathrm{high}} = T_0$ and $T_{\mathrm{low}} = T_L$) is chosen in order to examine the modeled TEG segregated from the feedback on the heat source and sink. Therefore, the results of the transient distributed-properties models from Section II-B and C can be compared with those delivered by a simple static averaged-properties (StAP) model.[1] The StAP model does not use intermediate temperatures and operates with constant α, λ, and r calculated for the average temperature $\overline{T} = (T_0 + T_L)/2$.

[1]In the StAP model, the entire p-legs and n-legs are each represented by *one* reduced segment model according to Fig. 1(d), where the component "heatCap" is removed and "TE_Voltage" calculates $dU_{\mathrm{th}} (= U_{\mathrm{th,Leg}})$ from the overall average temperature $(T_0 + T_L)/2$.

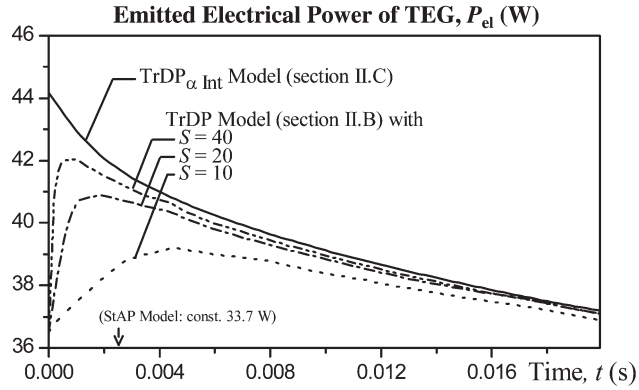

Fig. 6. Initial transient phase of Fig. 5: inaccurate behavior of the TrDP model due to extreme initial temperature gradient (cf., Fig. 2; *setting 1*).

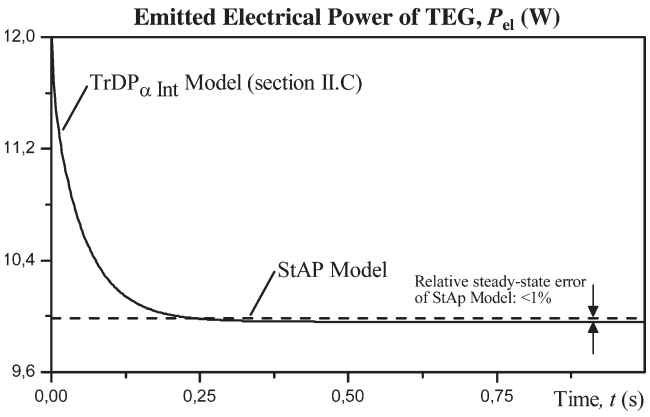

Fig. 7. Simulation of system model from Fig. 4 ($T_{\mathrm{high}} = 400$ K and $T_{\mathrm{low}} = 300$ K): exemplary setting with small steady-state deviation between the TrDP$_{\alpha\mathrm{Int}}$ model and the StAP model (*setting 2*).

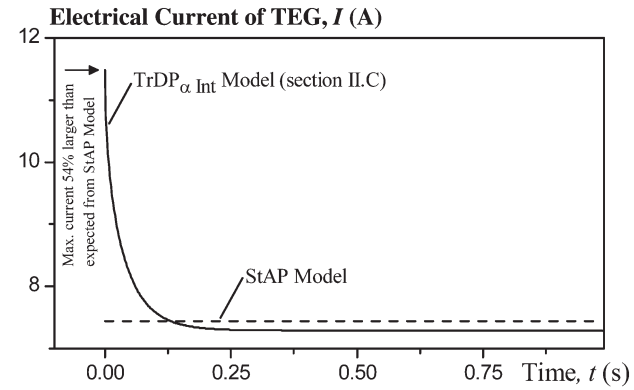

Fig. 8. Simulation of system model from Fig. 4 ($T_{\mathrm{high}} = 500$ K and $T_{\mathrm{low}} = 300$ K; **short circuit**, i.e., $R = 0$): comparison between the TrDP$_{\alpha\mathrm{Int}}$ model and the StAP model (*setting 3*).

In the following, the results of *step responses* are discussed, where the complete TEG is initially cooled down to the cold-side boundary temperature $T(x, 0) = T_{\mathrm{low}} = 300$ K. At time $t = 0^+$, the hot side is exposed to T_{high}. All simulations were performed by Dymola 7. The results show that the inaccuracy of the simple StAP model depends on the respective setting and is difficult to predict.

Setting 1: The load resistor is chosen to obtain maximal electric power in steady state, i.e., it matches the steady-state resistance of the TEG ($R = 2.502\ \Omega$), and T_{high} is set to 500 K. The dynamic model is the TrDP$_{\alpha\mathrm{Int}}$ model according

TABLE I
STATIC VALIDATION OF TrDP$_{\alpha\mathrm{Int}}$ AND StAP MODELS FOR LOAD VOLTAGE

	Datasheet	TrDP$_{\alpha\ \mathrm{Int}}$		StAP	
Type	U_{L} (V)	U_{L} (V)	Error(%)	U_{L} (V)	Error(%)
127-200-9	2.808	2.782	−0.93	2.800	−0.28
199-200-5	4.320	4.362	+0.97	4.391	+1.64
254-200-7	5.508	5.568	+1.09	5.608	+1.82
287-150-16	6.534	6.29	−3.73	6.336	−3.03

TABLE II
STATIC VALIDATION OF TrDP$_{\alpha\mathrm{Int}}$ AND StAP MODELS FOR LOAD CURRENT

	Datasheet	TrDP$_{\alpha\ \mathrm{Int}}$		StAP	
Type	I_{L} (A)	I_{L} (A)	Error(%)	I_{L} (A)	Error(%)
127-200-9	0.596	0.591	−0.84	0.594	−0.34
199-200-5	1.726	1.743	+0.98	1.755	+1.68
254-200-7	0.542	0.548	+1.11	0.552	+1.85
287-150-16	0.480	0.462	−3.75	0.465	−3.12

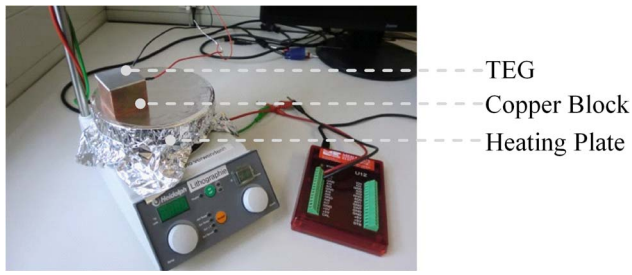

Fig. 9. Test setup according to Section IV-B.

to Section II-C with $S = 10$ discretization steps (increasing S will hardly change the results of the TrDP$_{\alpha\mathrm{Int}}$ model in the examples). Fig. 5 shows that the electric power output of the StAP model deviates from the TrDP$_{\alpha\mathrm{Int}}$ model by 11%; in the transient phase, deviations can be even bigger. The initial overshoot of P_{el} (due to the lower resistance of the cold TEG) cannot be reproduced by the static model. In the temperature range from 300 to 500 K, the nonlinearities of the TE material properties (cf., Fig. 3) obviously have a significant effect. The zoom in Fig. 6 reveals that, in the very early transient phase, the TrDP model is also imprecise, even with high spatial resolution; here, the TrDP$_{\alpha\mathrm{Int}}$ model is preferable. In the subsequent time, the TrDP model quickly tends to become the TrDP$_{\alpha\mathrm{Int}}$ model. This also holds for the following simulations, where the results of the TrDP model are omitted.

Setting 2: The steady-state deviation of the StAP model turns out to be negligible if the considered TEG operates between 300 and 400 K (cf., Fig. 7), where its $\alpha(T)$ and $\lambda(T)$ are approximately constant and $r(T)$ increases almost linearly.

Setting 3: This shows the short-circuit case ($R = 0\ \Omega$), which might occur accidentally as well as systematically by a high capacitive load. Here, the initially cold TEG produces the highest overshoot of the initial current (if the short-circuit inductivity is negligible). Due to the broad temperature range ($T_{\mathrm{high}} = 500$ K and $T_{\mathrm{low}} = 300$ K), the maximal initial current given by the TrDP$_{\alpha\mathrm{Int}}$ model is actually 54% higher than the estimation by the simpler StAP model (cf., Fig. 8).

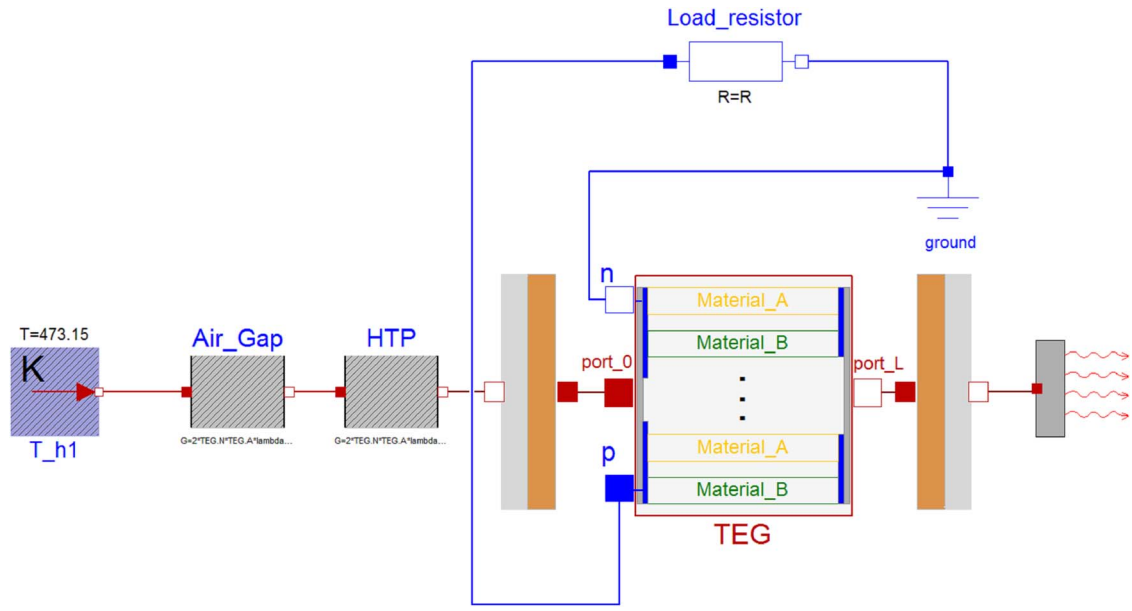

Fig. 10. Extended Modelica model of the experimental setup.

Of course, these quantitative results are only true for the considered setup and TE material properties. The required precision and the importance of the rather short transient behavior depend on the application. In general, the transient behavior is useful to quantify the reaction to sudden fluctuations in the boundary conditions. In thicker TE devices (i.e., longer leg length L), the transient effects fade slower, but in return, the device's thermal sensitivity is decreased.

IV. Experiment and Validation

A. Static Validation

To validate the steady-state behavior, the developed models (StAP and TrDP$_{\alpha\mathrm{Int}}$) are compared with data given by manufacturer datasheets [43]. Besides geometrical information, used as model parameters, the datasheets for different TEGs give data for the load voltage and current. The different types vary in the number of thermocouples and in the geometrical size of the TE legs. This information has validity for a temperature difference of 100 K, where the hot side is at 423.15 K. Table I shows the correctness of load voltage (R = internal resistance of TEG) for both models. For similar reasons as in setting 2, the difference between the two models is negligible.

The results for the internal resistance (not given in this paper) show major differences of up to 60%. It can be assumed that this is due to the neglected contact resistances between the thermocouples (up to 287). If the value of the internal resistor is corrected, the static validation for the load current (Table II) shows the correctness of the models.

B. Dynamic Validation

The test setup for the dynamic validation (Fig. 9) follows the step response scenario of Section III: an initially cooled TEG is instantaneously placed on the hot surface of a copper block. A TEG 199-200-5 of Thermalforce with a load resistance of 2.7 Ω (internal plus resistance between the contacts) is used. A temperature-controlled heating plate acts as heat source. A measurement PC logs the voltage over the resistance.

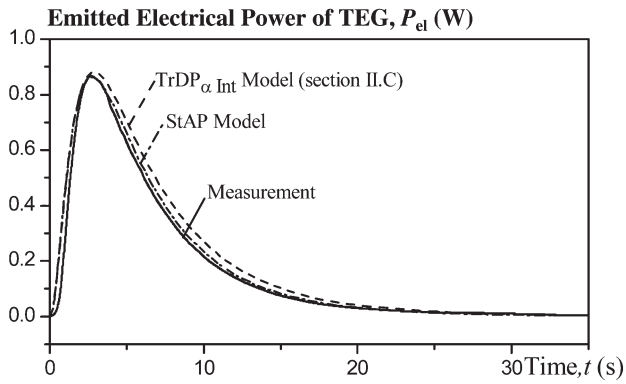

Fig. 11. Comparison of the arithmetic average of three series of measurements with the two different TEG models.

The arithmetic average of three series of measurements is compared with the simulation result. To allow this comparison, the Modelica model of the TEG from Fig. 4 is extended by the surrounding ceramic plates, the heat transfer paste, and an air gap as shown in Fig. 10.

A comparison with the different TEG models is shown in Fig. 11. The results of the simulation models are in good accordance with the measurements. Fig. 11 does not show the step response of the pure TE material but the dynamic behavior for the complete TEG (including ceramics). Because of the inert behavior of the peripheral components, the dynamics of the TEG has less effect.

V. Conclusion and Outlook

This paper has described a transient 1-D spatially resolved simulation model for TE legs, named TrDP/TrDP$_{\alpha\mathrm{Int}}$ model. The model is systematically derived from the governing partial

differential equations. It can be parameterized by lookup tables of the temperature-dependent TE material properties. Based on the generic TE leg model, models of TE power devices (TEGs or Peltier coolers) can be easily composed.

The model is implemented in a component-oriented way by means of the *modeling language Modelica*. On the one hand, this preserves the physical structure in the composition of a system model. On the other hand, the modeling scheme facilitates integrating the TE model into a system of other reusable models describing the heat sources, heat transfer, and appropriate power electronics (cf., e.g., [36] and [37]).

The TE models can be used to evaluate a conceived system design and can help optimize its performance. Indeed, not every design application will require the precision of the proposed TrDP/TrDP$_{\alpha\mathrm{Int}}$ model. However, given the varying superposition of diverse temperature-dependent effects, the lost accuracy of a simpler static averaged-properties model (StAP model) is difficult to quantify. The comprehensive integration of the TE phenomena makes the proposed model largely independent of the application and the precision required. Due to their genericity, all of the presented models can be integrated into a Modelica system model without reconsidering the implemented details of thermoelectricity.

In the highly topical field of waste heat recovery by means of TEGs, the long-term prediction of a planned system's profitability, is another important issue. For this purpose, the physical models have to be complemented with appropriate economic components including time-dependent government subsidies, e.g., in the same way as it was illustrated for an organic rankine cycle (ORC) plant in [34]. In [42], the presented TE models and the economic components from [34] are used to compare the predicted lifecycle profitability of a TEG-based waste heat recovery system with that of an ORC system.

The Modelica model and library is available on request at the Chair of Automation, Saarland University, Saarbrücken, Germany.

REFERENCES

[1] A. Tay, H. T. Chua, Y. Wang, and Y. S. Ngo, "Equipment design and control of advanced thermal processing module in lithography," *IEEE Trans. Ind. Electron.*, vol. 57, no. 3, pp. 1112–1119, Mar. 2010.

[2] J. P. Carmo, L. M. Gonçalves, and J. H. Correia, "Thermoelectric microconverter for energy harvesting systems," *IEEE Trans. Ind. Electron.*, vol. 57, no. 3, pp. 861–867, Mar. 2010.

[3] P. Nenninger and M. Ulrich, "Feasibility of energy harvesting in industrial automation wireless networks," in *Proc. 18th IFAC World Congr.*, 2011, pp. 13 888–13 892.

[4] S. Dalola, M. Ferrari, V. Ferrari, M. Guizzetti, D. Marioli, and A. Taroni, "Characterization of thermoelectric modules for powering autonomous sensors," *IEEE Trans. Instrum. Meas.*, vol. 58, no. 1, pp. 99–107, Jan. 2009.

[5] A. Moser, M. Erd, M. Kostic, K. Cobry, M. Kroener, and P. Woias, "Thermoelectric energy harvesting from transient ambient temperature gradients," *J. Electron. Mater.*, vol. 41, no. 6, pp. 1653–1661, Jun. 2012.

[6] M. E. Kiziroglou, S. W. Wright, T. T. Toh, P. D. Mitcheson, T. Becker, and E. M. Yeatman, "Design and fabrication of heat storage thermoelectric harvesting devices," *IEEE Trans. Ind. Electron.*, vol. 61, no. 1, pp. 302–309, 2014.

[7] D. M. Rowe, J. Smith, G. Thomas, and G. Min, "Weight penalty incurred in thermoelectric recovery of automobile exhaust heat," *J. Electron. Mater.*, vol. 40, no. 5, pp. 784–788, May 2011.

[8] K. T. Chau and C. C. Chan, "Emerging energy-efficient technologies for hybrid electric vehicles," *Proc. IEEE*, vol. 95, no. 4, pp. 821–835, Apr. 2007.

[9] K. T. Zorbas, E. Hatzikraniotis, and K. M. Praskevopoulos, "Power and efficiency calculation in commercial TEG and application in wasted heat recovery in automobile," presented at the 5th Eur. Conf. Thermoelectrics, Odessa, Ukraine, 2007, Paper 30.

[10] T. H. Braig and J. Ungethüm, "System-level modeling of an ice-powered vehicle with thermoelectric waste-heat-utilization," in *Proc. 7th Int. Modelica Conf.*, 2009, pp. 708–715.

[11] N. Phillip, O. Maganga, K. J. Burnham, J. Dunn, C. Rouaud, M. A. Ellis, and S. Robinson, "Modelling and simulation of a thermoelectric generator for waste heat energy recovery in low carbon vehicles," in *Proc. 2nd Int. Symp. EFEA*, 2012, pp. 94–99.

[12] D. Platzek, G. Bastian, K.-H. Förderer, D. Tatarinov, A. Vogelsang, H. Hupe, H. Platzek, M. Niecknig, and M. Preller, "A thermoelectric power generator for the metalworking industry," presented at the 28th Int. Conf. Thermoelectrics, Freiburg, Germany, 2009.

[13] S. Maneewan and S. Chindarsksa, "Thermoelectric power generation system using waste heat from biomass drying," *J. Electron. Mater.*, vol. 38, no. 7, pp. 974–980, Jul. 2009.

[14] B. I. Ismail and W. H. Ahmed, "Thermoelectric power generation using waste-heat energy as an alternative green technology," in *Recent Patents on Electrical Engineering*. Sharjah, UAE: Bentham Sci. Publ. Ltd., 2009, pp. 27–39.

[15] D. M. Rowe, "Thermoelectric waste heat recovery as a renewable energy source," *Int. J. Innovations Energy Syst. Power*, vol. 1, no. 1, pp. 13–23, Nov. 2006.

[16] L. Li, Z. Chen, M. Zhou, and R. Huang, "Developments in semiconductor thermoelectric materials," *Frontiers Energy*, vol. 5, no. 2, pp. 125–136, Jun. 2011.

[17] H. J. Goldsmid, *Introduction to Thermoelectricity*. Berlin, Germany: Springer-Verlag, 2010.

[18] J. D'Angelo, A. Downey, and T. Hogan, "Temperature dependent thermoelectric material power factor measurement system," *Rev. Sci. Instrum.*, vol. 81, no. 7, p. 075107, Jul. 2010.

[19] C. B. Vining, "An inconvenient truth about thermoelectrics," *Nat. Mater.*, vol. 8, no. 2, pp. 83–85, Feb. 2009.

[20] D. Narducci, "Do we really need high thermoelectric figures of merit? A critical appraisal to the power conversion efficiency of thermoelectric materials," *Appl. Phys. Lett.*, vol. 99, no. 10, pp. 102104-1–102104-3, Sep. 2011.

[21] T. Fujisaka and R. O. Suzuki, "Dimensional optimization in thermoelectric module for solar power generation," in *Proc. 38th Conf. IEEE Ind. Electron. Soc.*, Oct. 2012, pp. 5868–5872.

[22] R. O. Suzuki, Y. Sasaki, T. Fujisaka, and M. Chen, "Power generation using the fluids blown perpendicular to the TE panel," in *Proc. 38th Conf. IEEE Ind. Electron. Soc.*, Oct. 2012, pp. 5873–5888.

[23] S. Zhou, B. G. Sammakia, B. White, and P. Borgesen, "A multiscale modeling of thermoelectric generators for conversion efficiency optimization," in *Proc. 13th IEEE Intersoc. Conf. ITherm*, 2012, pp. 985–992.

[24] H.-L. Tsai and J.-M. Lin, "Model building and simulation of thermoelectric module using MATLAB/Simulink," *J. Electron. Mater.*, vol. 39, no. 9, pp. 2105–2111, Sep. 2010.

[25] D. T. Crane, "An introduction to system-level, steady-state and transient modeling and optimization of high-power-density thermoelectric generator devices made of segmented thermoelectric elements," *J. Electron. Mater.*, vol. 40, no. 5, pp. 561–569, May 2011.

[26] S. L. Lineykin and S. Ben-Yaakov, "Modeling and analysis of thermoelectric modules," *IEEE Trans. Ind. Appl.*, vol. 43, no. 2, pp. 505–512, Mar./Apr. 2007.

[27] I. Laird and D. D. C. Lu, "Spice steady state modelling of thermoelectric generators involving the Thomson effect," in *Proc. 37th Conf. IEEE Ind. Electron. Soc.*, 2011, pp. 1584–1589.

[28] M. O. Cernaianu, C. Cirstea, and A. Gontean, "Thermoelectrical energy harvesting system: Modelling, simulation and implementation," in *Proc. 10th ISETC*, 2012, pp. 67–70.

[29] N. Q. Nguyen and K. Pochiraju, "Behavior of thermoelectric generators exposed to transient heat sources," *Appl. Thermal Eng.*, vol. 51, no. 1/2, pp. 1–9, Mar. 2013.

[30] F. Felgner and G. Frey, "Object-oriented simulation model of thermoelectric devices for energy system design," in *Proc. 16th IEEE Mediterranean Electrotech. Conf.*, 2012, pp. 577–580.

[31] Website of the Modelica Association. [Online]. Available: http://www.modelica.org

[32] M. Tiller, *Introduction to Physical Modeling With Modelica*. Norwell, MA, USA: Kluwer, 2001.

[33] A. Cammi, F. Casella, M. Ricotti, and F. Schiavo, "Object-oriented modeling, simulation and control of the IRIS nuclear power plant with Modelica," in *Proc. 4th Int. Modelica Conf.*, 2005, pp. 423–432.

[34] F. Felgner, L. Exel, and G. Frey, "Component-oriented ORC plant modeling for efficient system design and profitability prediction," in *Proc. IEEE/IES Int. Conf. Clean Elect. Power*, 2011, pp. 196–203.
[35] C. Junior, C. Richter, W. Tegethoff, N. Lemke, and J. Köhler, "Modeling and simulation of a thermoelectric heat exchanger using the object-oriented library TIL," in *Proc. 6th Int. Modelica Conf.*, 2008, pp. 437–445.
[36] D. Cao and F. Z. Peng, "Multiphase multilevel modular dc–dc converter for high-current high-gain TEG application," *IEEE Trans. Ind. Appl.*, vol. 47, no. 3, pp. 1400–1408, May/Jun. 2011.
[37] R.-Y. Kim, J.-S. Lai, L. B. York, and A. Koran, "Analysis and design of maximum power point tracking scheme for thermoelectric battery energy storage system," *IEEE Trans. Ind. Electron.*, vol. 56, no. 9, pp. 3709–3716, Sep. 2009.
[38] M. Naji, M. Alata, and M. A. Al-Mimr, "Transient behaviour of thermoelectric device," *Proc. Inst. Mech. Eng., Part A: J. Power Energy*, vol. 217, no. 6, pp. 615–621, Sep. 2003.
[39] F. Felgner, R. Merz, and L. Litz, "Modular modelling of thermal building behaviour using Modelica," *Math. Comput. Modell. Dyn. Syst.*, vol. 12, no. 1, pp. 35–49, Feb. 2006.
[40] G. J. Snyder, "Application of the compatibility factor to the design of segmented and cascaded thermoelectric generators," *Appl. Phys. Lett.*, vol. 84, no. 13, pp. 2436–2438, Mar. 2004.
[41] Website of the Thermonamic Electronics Corp., Ltd., Jiangxi, China. [Online]. Available: www.thermonamic.com
[42] F. Felgner, L. Exel, and G. Frey, "Model-based design and validation of waste heat recovery systems," in *Proc. 2nd IEEE Int. Energy Conf. Exhib.*, 2012, pp. 265–270.
[43] Website of Thermalforce.de, Berlin, Germany. [Online]. Available: http://www.thermalforce.de/de/product/thermogenerator/

Felix Felgner (M'11) received the Diplom-Ingenieur (M.Sc.) degree in electrical engineering/control engineering and the Doktor-Ingenieur (Ph.D.) degree in electrical engineering/automation from the University of Kaiserslautern, Kaiserslautern, Germany, in 2002 and 2008, respectively.

He was a Research Assistant with the University of Kaiserslautern for six years. He has been a Postdoc with Saarland University, Saarbrücken, Germany, since 2009. His primary research interests are methodologies of modeling thermodynamics and energy systems as well as their application to design and control verification purposes.

Lukas Exel received the Diplom-Ingenieur (M.Sc.) degree in mechatronics engineering from Saarland University, Saarbrücken, Germany, in 2013.

Since then, he has been a Research Assistant with the Chair of Automation, Saarland University. As a Student Assistant, he was involved in research projects related to object-oriented modeling of organic rankine cycles. His diploma thesis deals with a forecasting system for supply-dependent feed-in units.

Marco Nesarajah received the Diplom-Ingenieur (M.Sc.) degree in mechatronics engineering from Saarland University, Saarbrücken, Germany, in 2013.

Since then, he has been a Research Assistant with the Chair of Automation, Saarland University. As a Student Assistant, he was involved in research projects related to the object-oriented modeling of thermoelectric devices. His diploma thesis deals with modeling and optimization of an organic rankine cycle plant.

Georg Frey (M'97–SM'07) received the Diplom-Ingenieur (M.Sc.) degree in electrical engineering/control engineering from Karlsruhe Institute of Technology, Karlsruhe, Germany, in 1996 and the Doktor-Ingenieur (Ph.D.) degree in electrical engineering/automation from the University of Kaiserslautern, Kaiserslautern, Germany, in 2002.

He was an Associate Professor with the University of Kaiserslautern and was also with the German Research Center for Artificial Intelligence (DFKI). Since 2009, he has been a Full Professor and holds the Chair of Automation, Saarland University, Saarbrücken, Germany. He is the author or coauthor of more than 160 peer-reviewed technical papers covering his research interests from modeling and simulation of complex automation and energy systems over the design and formal validation of logic control systems to development processes for distributed and safe automation systems.

Prof. Frey is the Cochair of the Information Technology in Industrial and Factory Automation Subcommittee of the IEEE/IES Technical Committee on Factory Automation.